Electronic Supplementary Material (ESI) for Journal of Materials Chemistry A.

True cable assembly with carbon nanotube sheath and nickel wire core: a fully flexible supercapacitor electrode integrating energy storage and electrical conduction

Huating Ye,[a,b] *Kai Wang,*[b] *Juntao Zhou,*[b] *Li Song,*[c] *Li Gu,**[*b] *and Xuebo Cao*[*c]

[a] School of Materials Science and Engineering, Changzhou University, Changzhou, Jiangsu 213164, PR China

[b] School of Materials and Textile Engineering, Jiaxing University, Jiaxing, Zhejiang 314001, PR China. E-mail: guli@mail.zjxu.edu.cn

[c] School of Biology and Chemical Engineering, Jiaxing University, Jiaxing, Zhejiang 314001, PR China. E-mail: xbcao@mail.zjxu.edu.cn

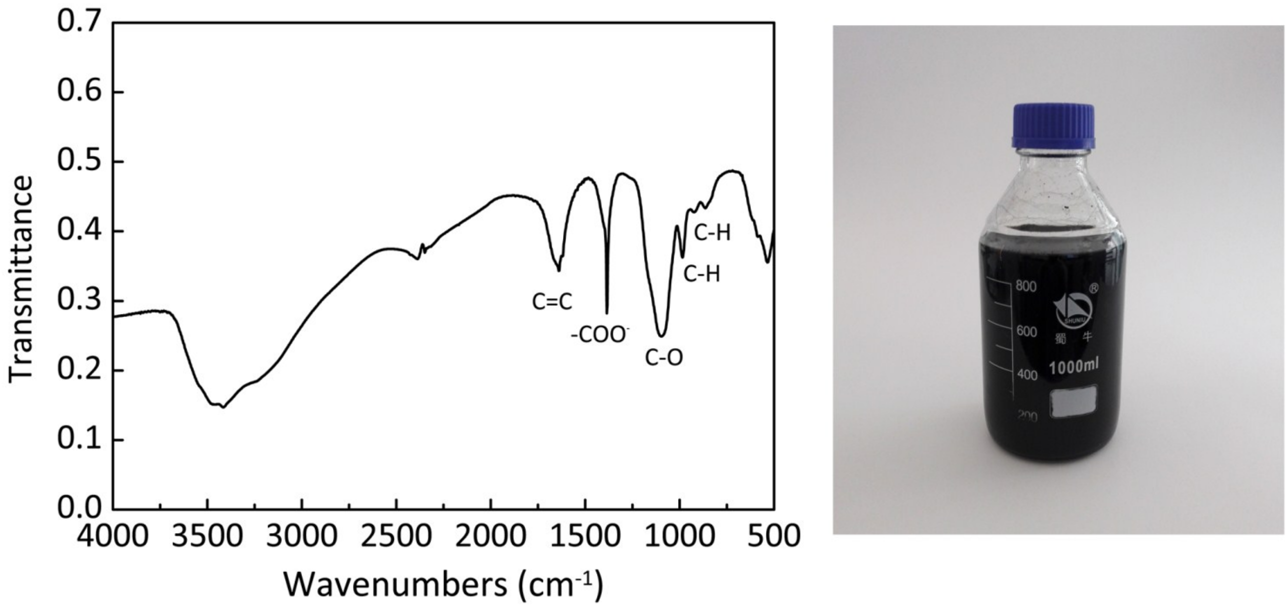

Fig. S1 Left: Fourier Transform Infrared spectrum for the acid-oxidized carbon nanotubes (CNTs). It shows the presence of oxygen-containing groups on the surfaces of the CNTs. Consequently, acid-oxidized CNTs can be homogeneously dispersed in water (right). Homogeneous CNTs solution is the prerequisite in assembling the cable with carbon nanotube sheath and nickel wire core

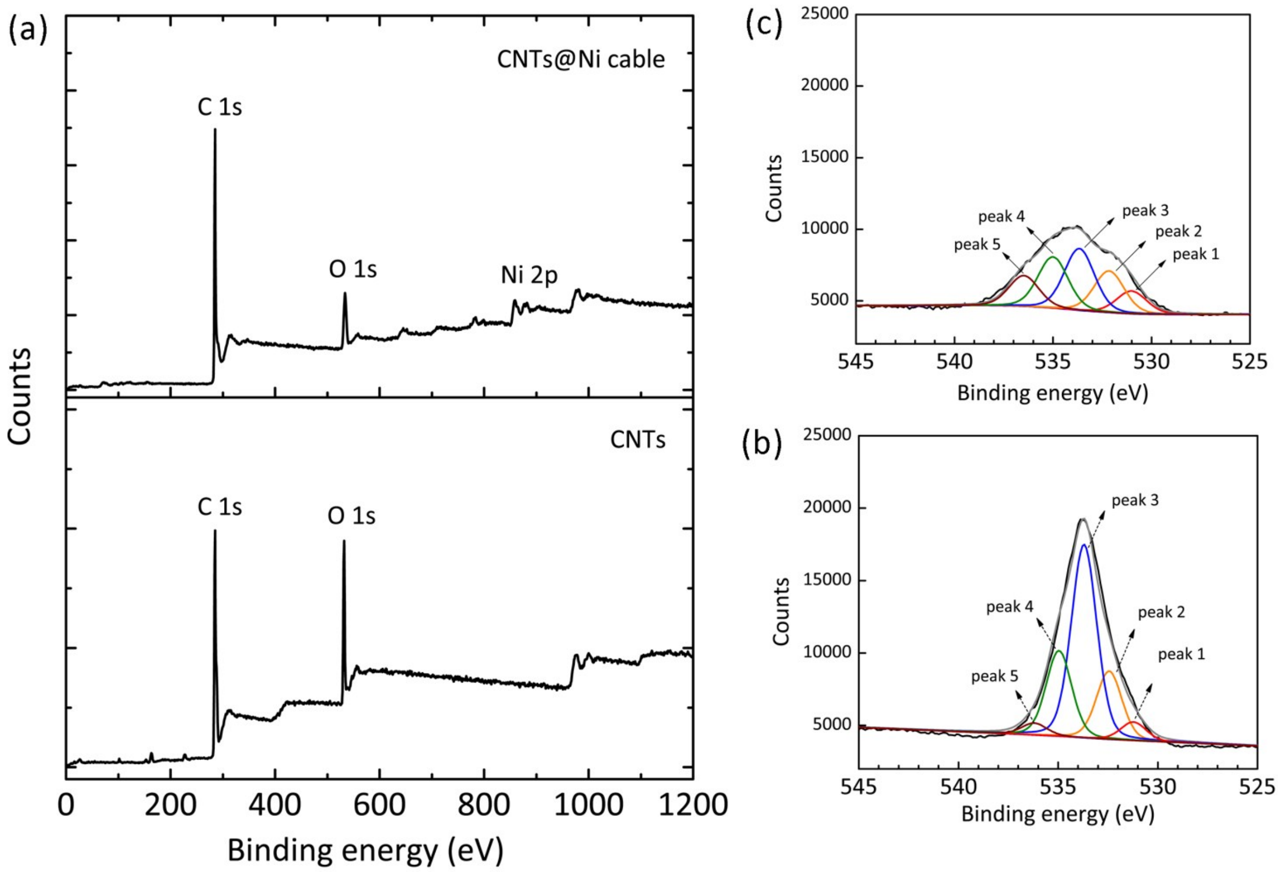

Fig. S2 (a) A comparison between the XPS surveying spectra for CNTs@Ni cable and the acid-oxidized MWCNTs for assembling the cable. (b) and (c) O 1s binding energy spectra for the acid-oxidized MWCNTs (b) and the CNTs@Ni cable (c). Peak 1 (530.9 eV), carbonyl oxygen; peak 2 (532.3 eV), oxygen atoms in hydroxyl groups; peak 3 (533.6 eV), ether-type oxygen atoms; peak 4 (534.9 eV), oxygen atoms in carboxyl groups; and peak 5 (536.5 eV), adsorbed water and/or oxygen.

It can be seen that the O1s signal is significantly reduced after the formation of the cable, which indicates that a portion of oxygen containing groups have been removed from the MWCNTs in the assembly process.

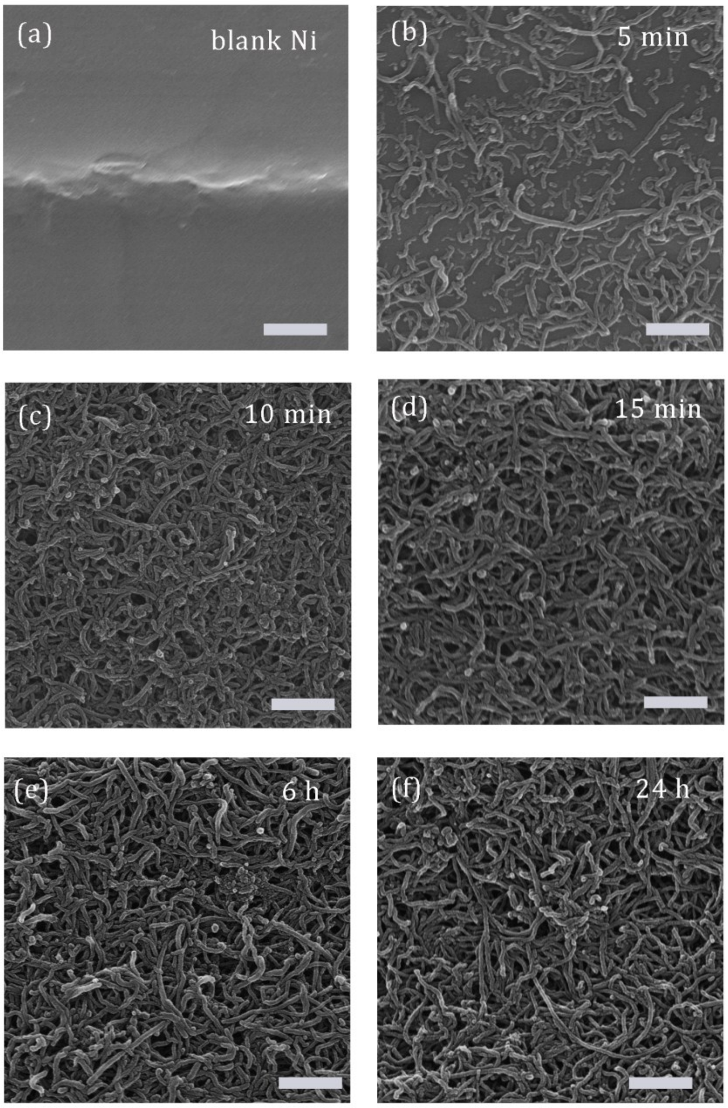

Fig. S3 SEM images taken on the surface of the cable with different growth time. Scale bars: 300 nm. It can be clearly seen that the surface of blank Ni wire is clean (a). After the interaction of Ni wire with the MWCNTs solution for only 5 min, CNTs like worms to wrap around the Ni wire (b). And 10 min later, the surface of the Ni wire has been completely covered by the CNTs (c), suggesting a rapid deposition rate of the MWCNTs and a high efficiency in the production of the CNTs@Ni cable.

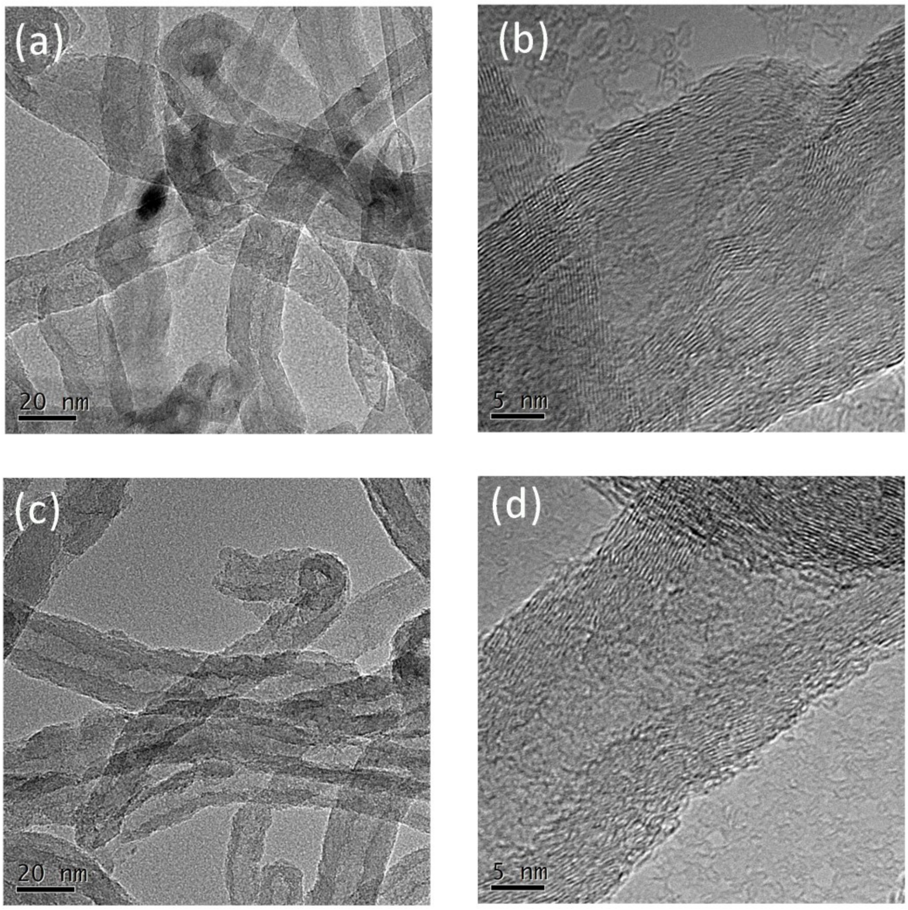

Fig. S4 (a, b) TEM images for the CNTs before the assembly. (c, d) TEM images the CNTs after the assembly on the Ni wire. For the preparation of the TEM sample, CNTs sheath was exfoliated from the cable by sonication and then dispersed in absolute ethanol. Next, a drop of the dispersion was dropped onto a carbon-coated copper grid. It can be seen that the tubular morphology of the CNTs was unchanged after the interaction with Ni^0 and the assembly process.

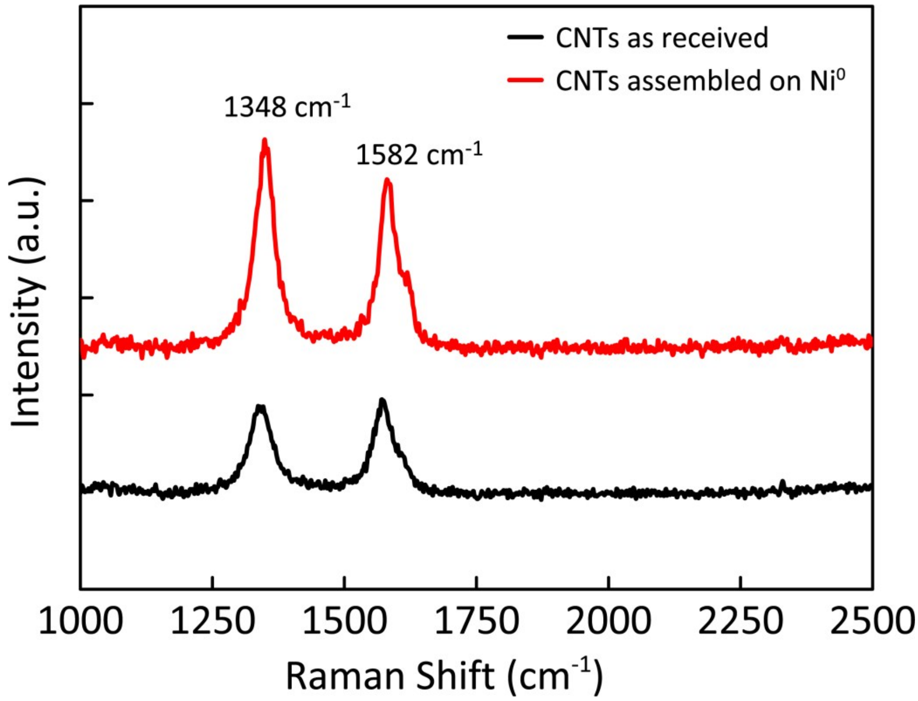

Fig. S5 Raman spectra for the CNTs before and after the assembly. They show two distinct peaks located at 1348 cm^{-1} and 1582 cm^{-1}, which are assigned to the characteristic D band (disorder and defects) and G band (graphitic), respectively. The higher intensity of D band for the CNTs assembled on the Ni^0 substrate is because an oxidization procedure has been applied to the CNTs prior to the assembly.

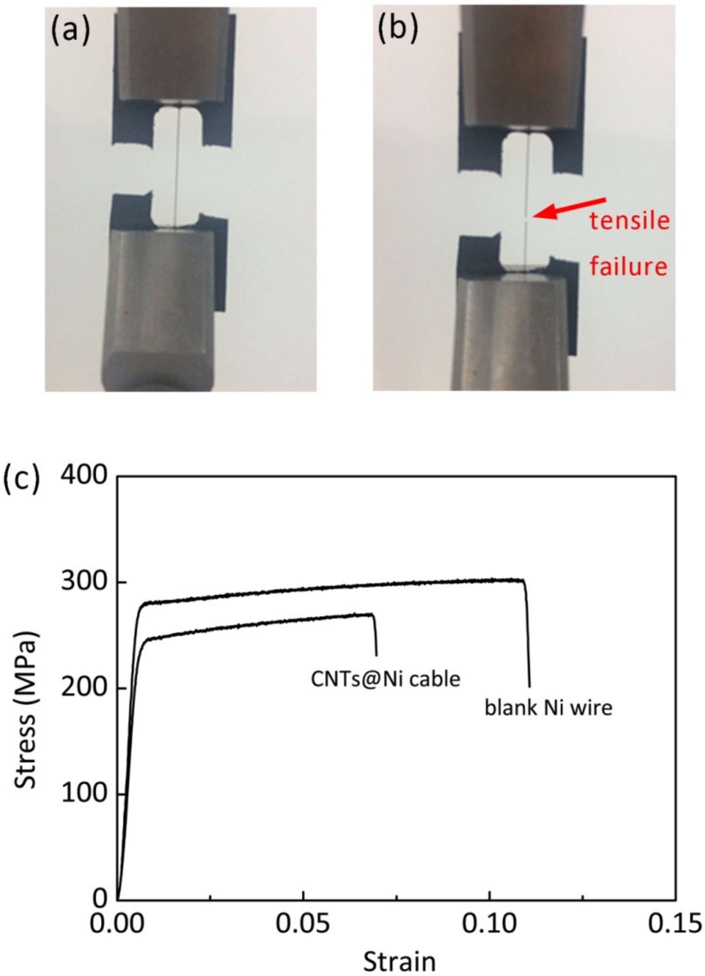

Fig. S6 Mechanical tests of blank Ni wire and the CNTs@Ni cable (diameter ~250 μm). (a, b) Photographs show the cable before and after the tensile failure. (c) Representative stress-strain curves of blank Ni wire and the CNTs@Ni cable, indicating high strength of the cable.

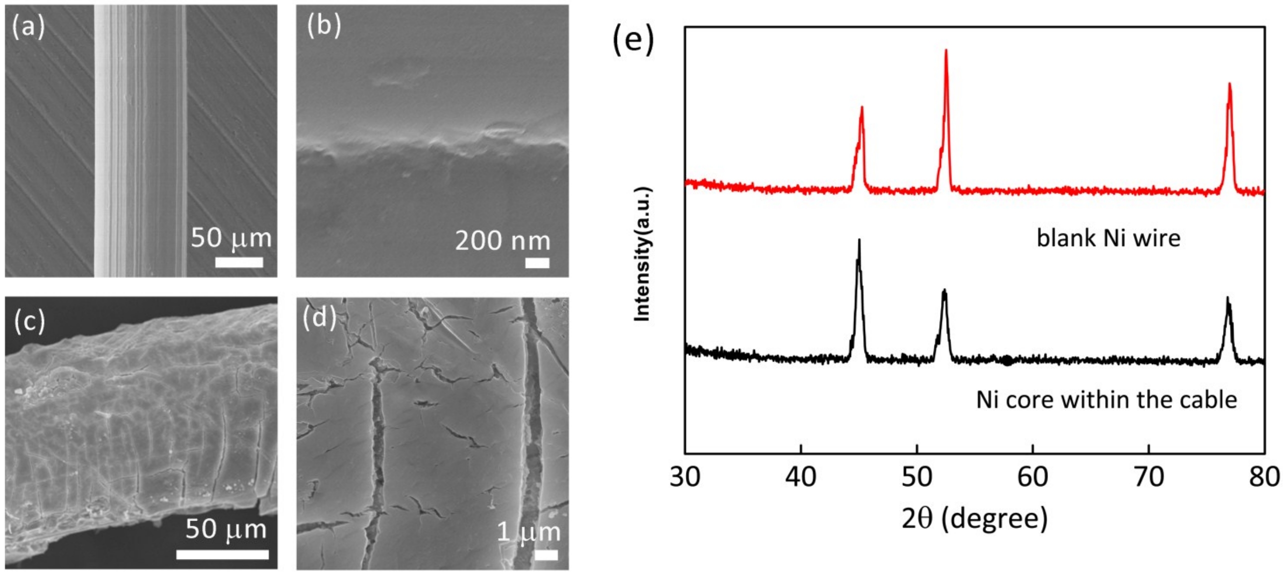

Fig. S7 (a, b) SEM images showing the surface of the Ni wire before the growth of the CNTs sheath. (c, d) SEM images showing the surface of the Ni core in the cable. For SEM characterization, CNTs sheath was exfoliated to expose the surface of the Ni core by sonication. (e) XRD patterns for the blank Ni wire and the Ni core in the cable. They suggest that the Ni core is still composed of elemental Ni.

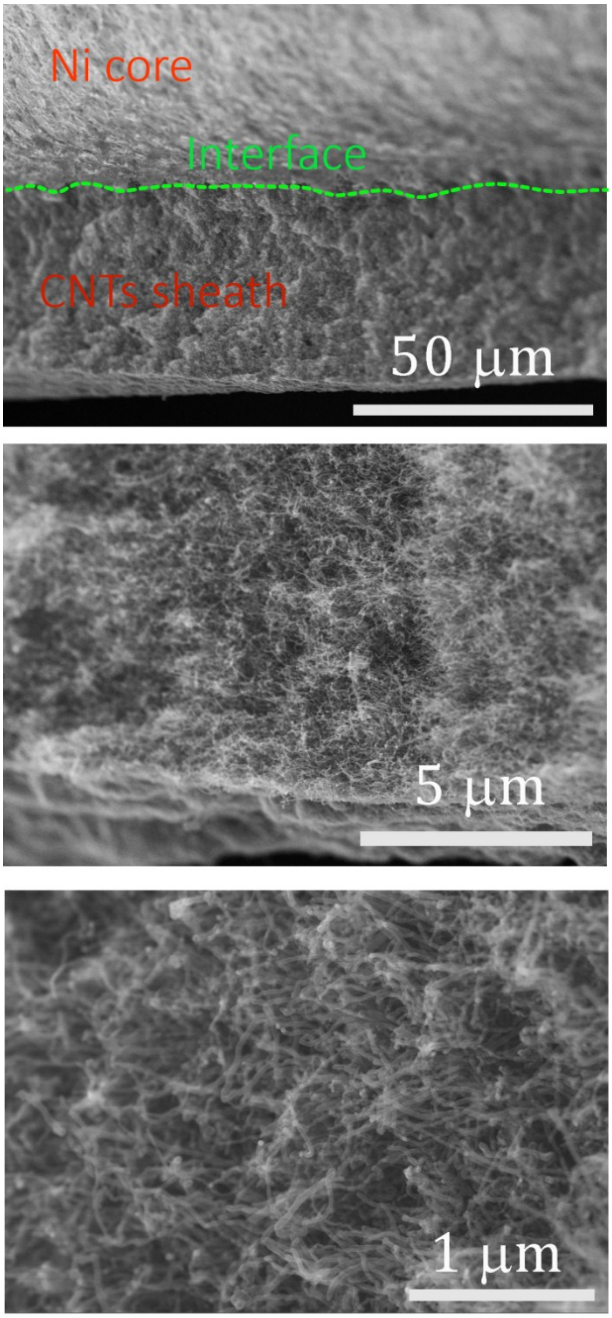

Fig. S8 SEM images show the interface between the CNTs sheath and the Ni wire core (top) and the nearly vertical alignment of the CNTs along the lateral axis of the Ni wire (middle and bottom). As seen, the CNTs sheath is dense, ordered, and free of defects. More importantly, there are no gaps at the interface between the sheath and the core, which reduces the charge transfer resistance.

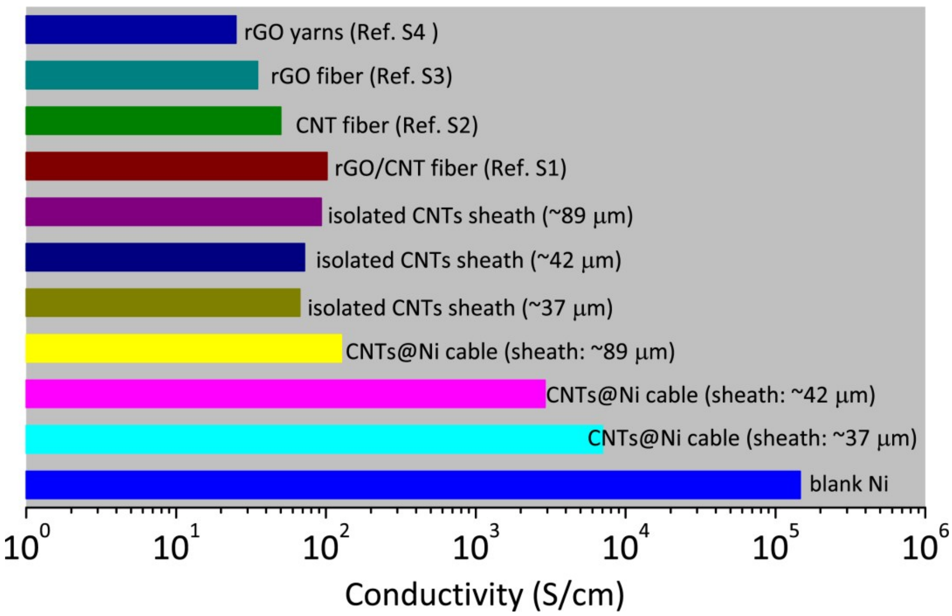

Fig. S9 A comparison in terms of conductivity of the result obtained in this work and the relevant examples reported in the literatures.

In order to measure the conductivity of isolated CNTs sheaths, the CNTs@Ni cables were soaked in 1 M FeCl3 solution to etch the Ni core ($Ni + 2Fe^{3+} == Ni^{2+} + 2Fe^{2+}$). After rinse with deionized water and absolute ethanol repetitively and drying, the conductivities of the CNTs sheaths were measured (silver paste as the contact). The CNTs sheathes with a thickness of 89 μm, 42 μm, and 37 μm show a conductivity of 93 S cm^{-1}, 72 S cm^{-1}, and 67 cm^{-1}, respectively. Such conductivities are typical for blank CNTs fibers. The much lower conductivity of isolated CNTs sheathes than CNTs@Ni cables is rational because of the removal of metallic Ni core that could transport electrons promptly. Meanwhile, the results may suggest that the presence of Ni is advantageous to the decrease of resistance and the application in electrode materials.

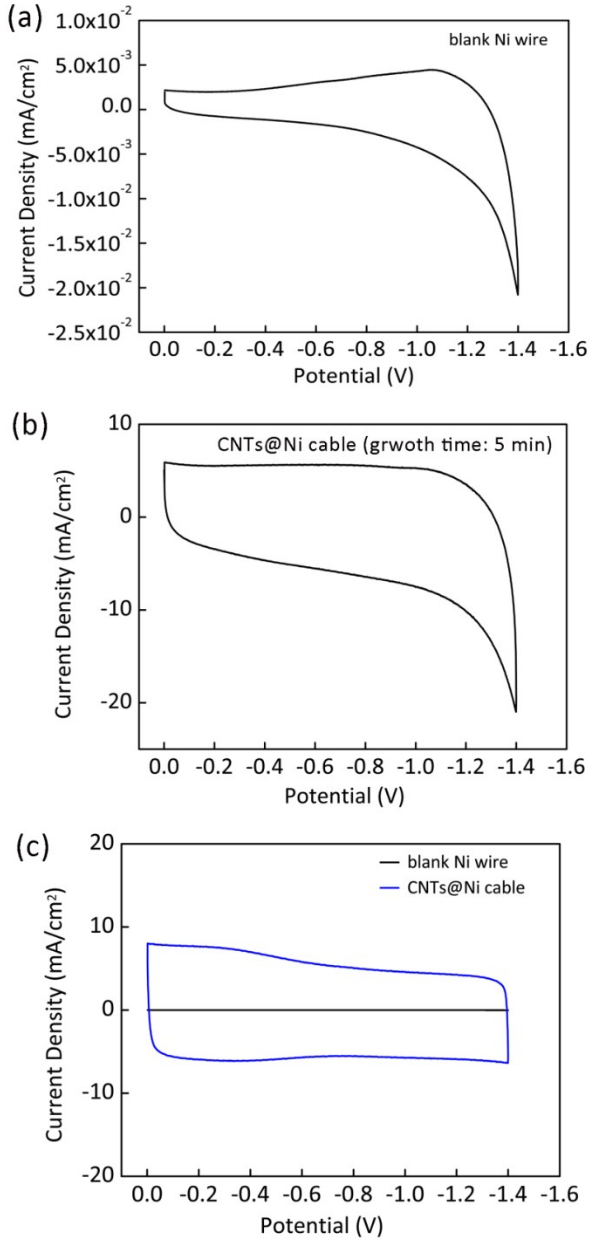

Fig. S10 (a) CV curve for the wire-shaped capacitor constructed by two blank Ni wires aligned in parallel. (b) CV curve for the wire-shaped capacitor constructed by two parallel CNTs@Ni cables with a growth time of 5 min (*see Figure S2b*). Both the CV curves in (a) and (b) reveal that, without the protection of the dense CNTs sheath, unwanted electrochemical reactions occurred because of the exposure of the Ni wire to the aqueous electrolyte. (c) A comparison between the CV profiles of blank Ni wire capacitor and CNTs@Ni cable capacitor, which demonstrates that the capacitance contribution from the Ni wire is inappreciable.

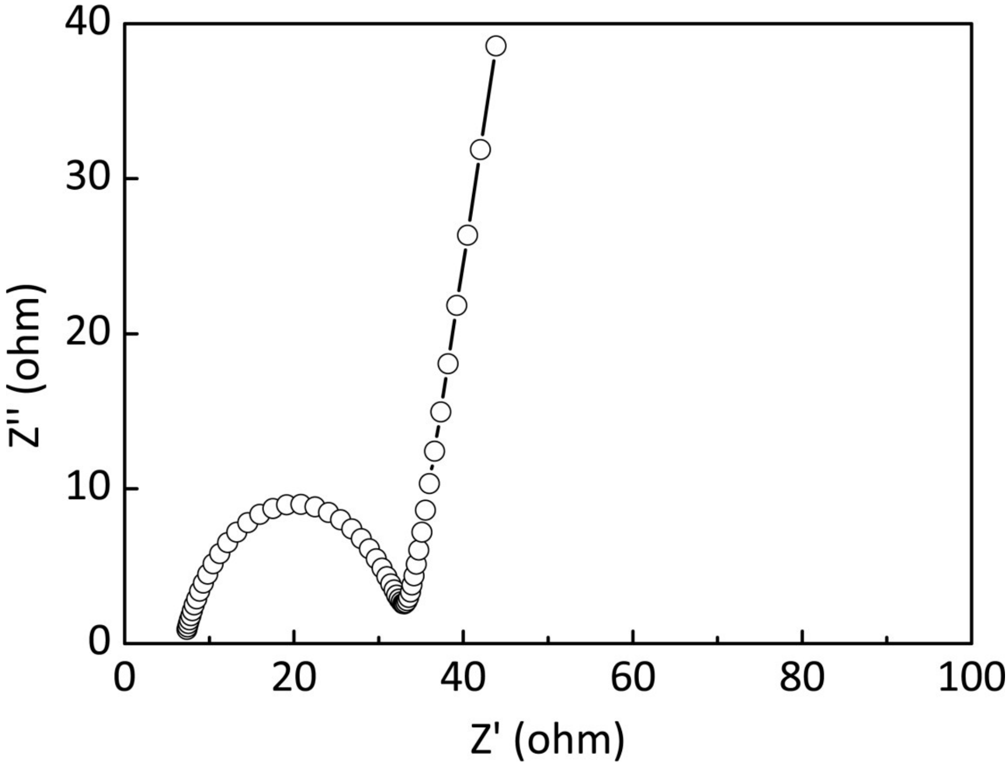

Fig. S11 Electrochemical impendence spectroscopy (EIS) characterization of the CNTs@Ni cable supercapacitor. According to recent analysis on the EIS spectra of the supercapacitors [S15], the span of the single semi-circle along the *x*-axis reflects the charge transfer resistance at the electrode/electrolyte interface, which is about 26 Ω. The *x*–intercept reflects the equivalent series resistance, which is estimated to be 7.5 Ω.

Table S1 Performance summary of recently reports on fiber-based supercapacitors

C_A (mF/cm^2)	C_V (mF/cm^3)	E_A (μWh/cm^2)	E_V (mWh/cm^3)	P_A (mW/cm^2)	P_V (mW/cm^3)	Refs.
117.1	13800	31.9	3.3-3.8	12.4	1590	this work
116.3	45000	--	6.3	--	1085	[S1]
39.7	--	1.77	--	0.043	--	[S5]
11.9-19.5	--	2.7	--	0.042-9.1	--	[S6]
35.67	--	10	2.16	7.3	1600	[S7]
1.2-1.7	--	0.04-0.17	--	0.006-0.1	--	[S8]
16.87	21210	0.46-1.25	0.58-1.57	0.2-1.65	260-2080	[S9]
2	--	0.27	--	0.014	--	[S10]
307	--	21.4	--	8.5	--	[S11]
19.4	1900	2.69	--	0.809	--	[S12]
177	15800	3.84	3.5	0.02	18	[S13]
86.8	--	9.8	--	0.189	--	[S14]

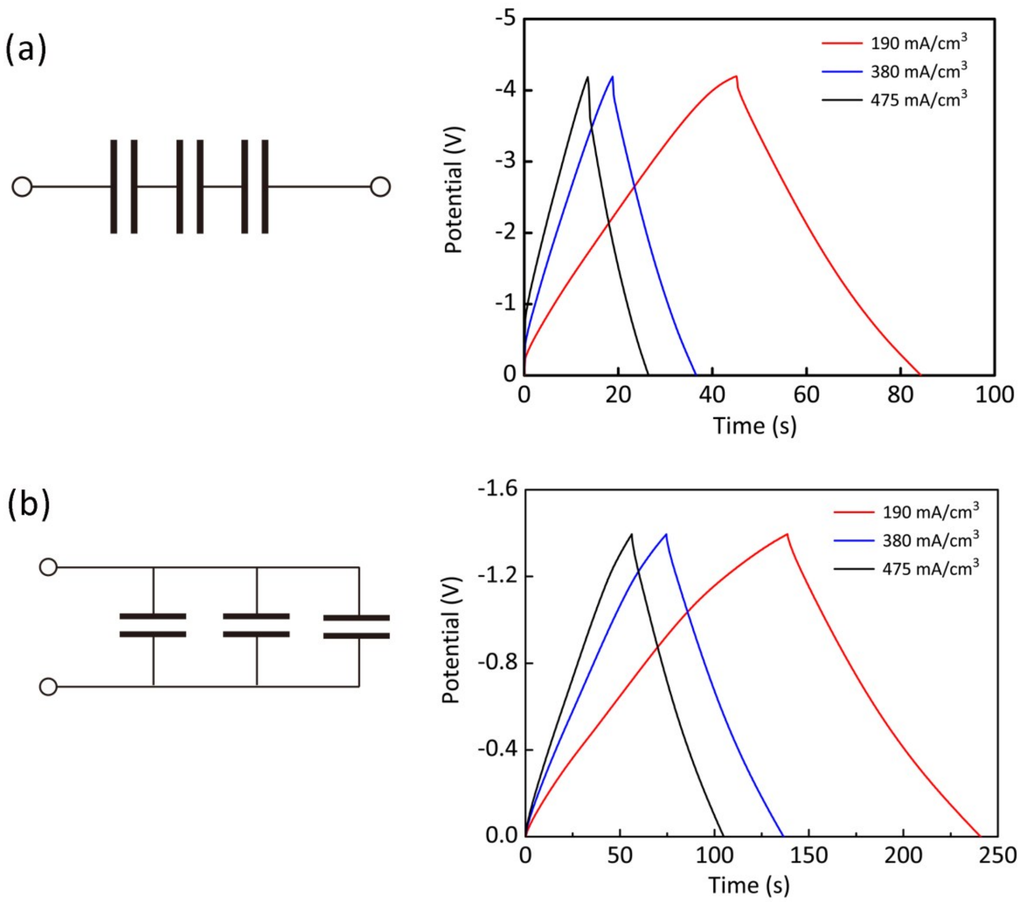

Fig. S12 GCD curves for the device group and the equivalent circuits. (a) Three in series. (b) Three in parallel.

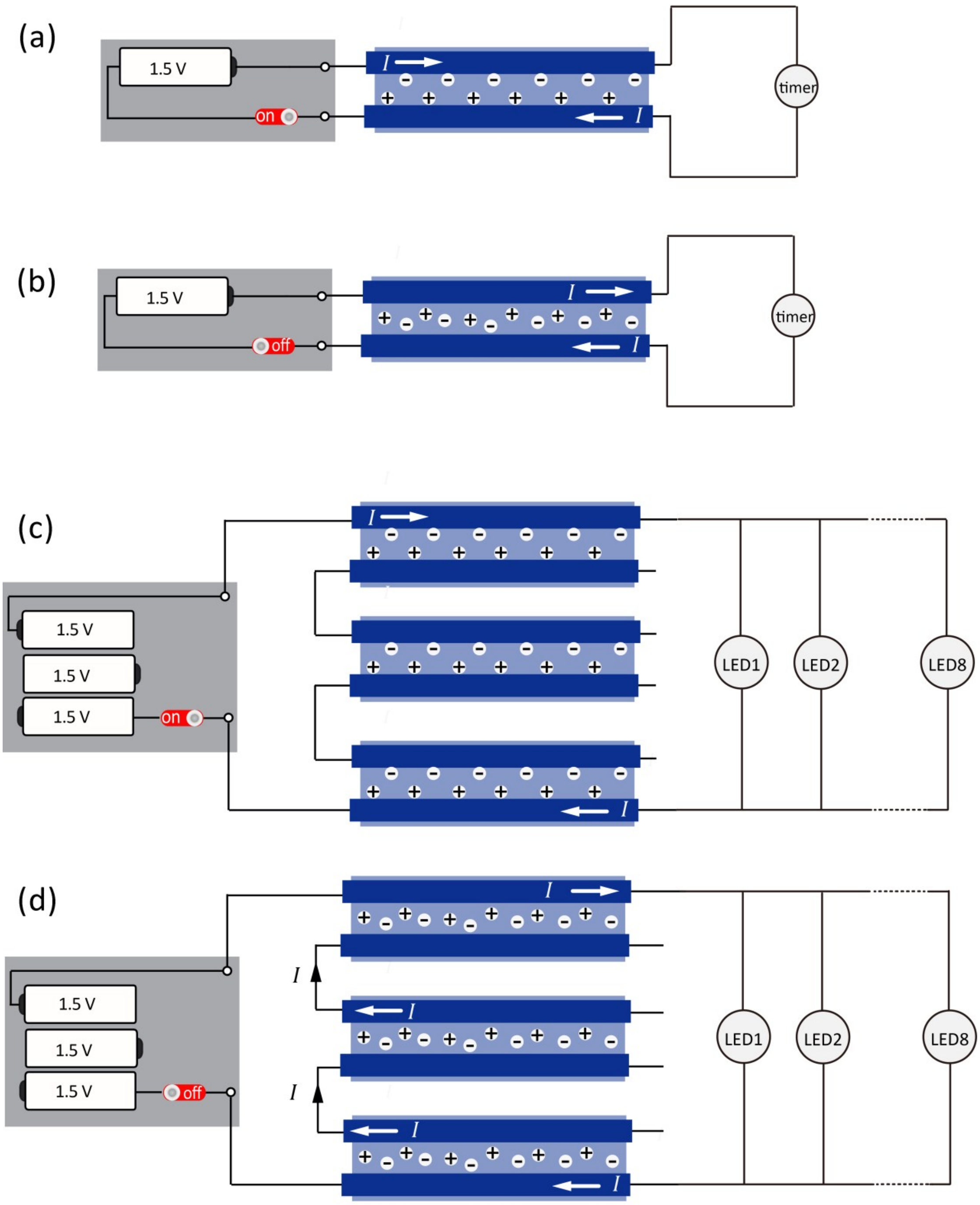

Fig. S13 Additional demo studies on the bi-functionality of the CNTs@Ni supercapacitor (*also see* **video S2** and **video S3** for details). (a-d) Equivalent circuits for demonstrating the integration of the energy transport and storage features into the CNTs@Ni supercapacitor. CNTs@Ni supercapacitors act as cable to connect the power source to the timer (a) or the LED array (c). CNTs@Ni supercapacitors act as power source to run the timer (b) or the LED array (d). In *a, b*, and Video S2, a single CNTs@Ni supercapacitor is used to power the timer. In *c, d*, and Video S3, a device group (three in connection) is used to light up the Letter “C”, “N”, or “T” consisting of LED array.

Reference

[S1] D. Yu, K. Goh, H. Wang, L. Wei, W. Jiang, Q. Zhang, L. Dai, Y. Chen, *Nat. Nanotechnol.* **2014**, 9, 555.

[S2] F. Gao, L. Viry, M. Maugey, P. Poulin, N. Mano, *Nature Commun.* **2010**, 1, 2.

[S3] H. P. Cong, X. C. Ren, P. Wang, S. H. Yu, *Sci. Rep.* **2012**, 2, 613.

[S4] S. H. Aboutalebi, R. Jalili, D. Esrafilzadeh, M. Salari, Z. Gholamvand, Y. S. Aminorroaya, K. Konstantinov, R. L. Shepherd, J. Chen and S. E. Moulton, *ACS Nano* **2016**, *8*, 2456.

[S5] J. Ren, W. Bai, G. Guan, Y. Zhang, H. Peng, *Adv. Mater.* **2013**, 25, 5965.

[S6] Y. Fu, X. Cai, H. Wu, Z. Lv, S. Hou, M. Peng, X. Yu, D. Zou, *Adv. Mater.* **2012**, 24, 5713.

[S7] X. Dong, Z. Guo, Y. Song, M. Hou, J. Wang, Y. Wang, Y. Xia, *Adv. Funct. Mater.* **2014**, 24, 3405.

[S8] Y. Meng, Y. Zhao, C. Hu, H. Cheng, Y. Hu, Z. Zhang, G. Shi, L. Qu, *Adv. Mater.* **2013**, 25, 2326.

[S9] P. Xu, B. Wei, Z. Cao, J. Zheng, K. Gong, F. Li, J. Yu, Q. Li, W. Lu, J. H. Byun, *ACS Nano* **2015**, 9, 6088.

[S10] J. Bae, M. K. Song, Y. J. Park, J. M. Kim, M. Liu, Z. L. Wang, *Angew. Chem. int. Ed.* **2011**, 50, 1683.

[S11] Y. Cao, M. Zhu, P. Li, R. Zhang, X. Li, Q. Gong, K. Wang, M. Zhong, D. Wu, F. Lin, H. Zhu, *Phys. Chem. Chem. Phys.* **2013**, 15, 19550.

[S12] P. Sun, R. Lin, Z. Wang, M. Qiu, Z. Chai, B. Zhang, H. Meng, S. Tan, C. Zhao, W. Mai, *Nano Energy* **2017**, 31, 432.

[S13] L. Kou, T. Huang, B. Zheng, Y. Han, X. Zhao, K. Gopalsamy, H. Sun, C. Gao, *Nature Commun.* **2014**, 5, 3754.

[S14] V. T. Le, H. Kim, A. Ghosh, J. Kim, J. Chang, Q. A. Vu, D. T. Pham, J. H. Lee, S. W. Kim, Y. H. Lee, *ACS Nano* **2013**, 7, 5940.